JOURNAL OF OPTOELECTRONICS AND ADVANCED MATERIALS, Vol. 11, No. 3, March 2009, p. 229 - 237

Review Paper

Magnetic materials for technical applications[a)]

E. BURZO[a,b*], M.M. CODESCU[b,c], W. KAPPEL[b,c], E. HELEREA[d]
[a] *Faculty of Physics, Babes-Bolyai University RO-400084 Cluj-Napoca, Romania*
[b] *SRMM – Bucharest, Romania*
[c] *INCDIE ICPE – CA Bucharest, Romania*
[d] *Transilvania University, Brasov, Romania*

The time evolution of the physical properties of hard and soft magnetic materials is shortly reviewed. Then, we analyse the magnetic properties of $Nd_5Fe_{67}Cr_8Nb_2B_{18}$ nanocomposites, Nd–Fe–Co–Al–B hard magnetic phases and magnets as well as of $Nd_2Fe_{14-x}M_xC_{0.8}B_{0.2}$ (M=Ni, Cu and Al) alloys. Some data on soft magnetic materials are also given. Finally, the magnetocaloric properties of ternary Gd–Co–B compounds are reported.

(Received December 15, 2008; after revision February 28, 2008; accepted March 19, 2009)

Keywords: Nanocrystalline alloys, Hard and soft magnetic materials, Magnetocaloric effect

1. Introduction

The magnetic materials have a wide range of applications being the main components in a large varieties of devices used in technical and social life. The increase of their performances was the main task of researches performed at the international level. New hard, semi–hard and soft magnetic materials were developed. The relative weight of magnetic materials, manufactured in the recent years are plotted in Fig. 1. High performance materials, recently elaborated, grow continuously as importance, particularly those in information technology. In addition, magnetocaloric effects showed by some systems, are now used in magnetic refrigeration technology.

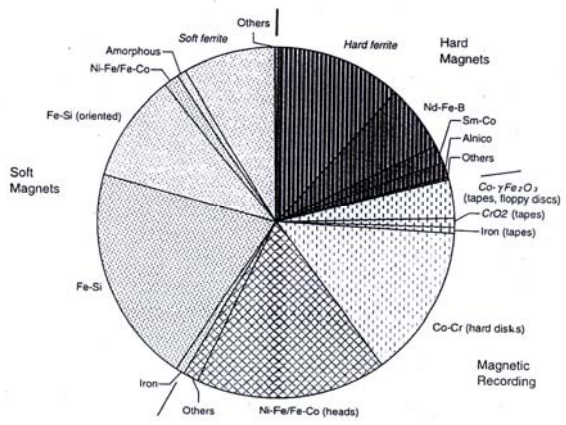

Fig.1 The relative weight of magnetic materials manufactured at the world scale.

The evolution of the coercive fields for hard and soft magnetic materials, during last 200 years, is shown in –Fig.2. Hard magnetic materials with coercivities higher than 10^7 A/m were now obtained, particularly by using rare–earth–transition metal compounds. The elaboration of high energy permanent magnets started in 1967 year, when $SmCo_5$–type magnets were obtained and continued to discovery in 1984 of Nd–Fe–B magnets. The relative inexpensive nanocomposites $Nd_2Fe_{14}B/\alpha$–Fe or $Nd_2Fe_{14}B/Fe_3B$ were then elaborated.

New soft magnetic materials were obtained with very low coercive fields and low magnetic losses as well as magnetocaloric alloys which now are used in refrigeration technology.

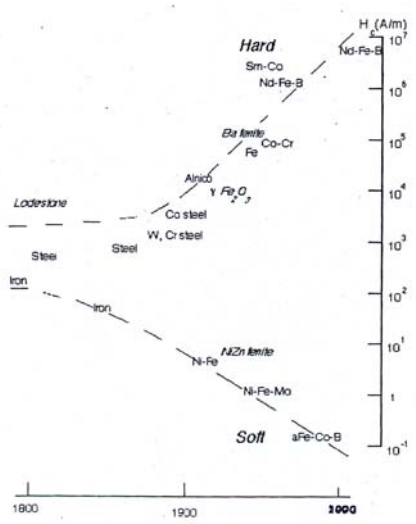

Fig.2 The time evolution of the coercive fields for hard and soft magnetic materials.

[a)] **based on lecture given at MATEHN International Conference**

In the followings we present some results obtained on nanocomposite systems based on $Nd_2Fe_{14}B/\alpha$–Fe, Nd–Fe–Co–Al–B, Nd–Fe–C alloys, Finemet–type low coercive materials as well as magnetocaloric properties Gd–Co–B based systems.

2. Magnetic properties of Nd–Fe–B nanocomposites

The Nd–Fe–B permanent magnets, having higher energy product than those based on Sm–Co were elaborated since 1984 [1]. Their hard magnetic properties are determined by $Nd_2Fe_{14}B$ phase. Although in this compound, from 17 atoms per formula unit, only boron is non magnetic, the Curie temperature is rather low, $T_c \cong 584$ K. Consequently, these magnets can be used only in a limited temperature range above the room temperature. Many researches were devoted to analyse the effect of various substitutions, at the iron sites, in increasing performances at higher temperatures [2–4]. The effect of complex substitutions as (Co+Al) was shown to be useful and will be discussed further.

Generally, the rare–earth metals are expensive, their abundance in terrestrial crust being of the order of ppm. A way to obtain cheaper magnets based on Nd–Fe–B was to realize nanocomposite systems [5]. These are formed from two magnetic phases, one hard, as $Nd_2Fe_{14}B$, and another soft (α–Fe or Fe_3B). The nanocomposite magnets prepared by both melt spinning and mechanical alloying, which are the main ways to be obtained, are isotropic. There is a difference between the predicted and actual energy product. The high value of the remanence ratio was attributed to the exchange coupling at the interface of the hard and soft magnetic nanograins. The exchange length for the soft phase, l_c, is given by $l_c=\pi(A/2K)^{1/2}$, where A is the exchange constant of the soft magnetic phase and K is the magnetocrystalline energy constants of the hard magnetic phase [6]. In the $Nd_2Fe_{14}B/\alpha$–Fe based nanocomposites, l_c =10–12 nm, depending on the substitutions performed at Fe sites in hard magnetic phase. The difference between the determined and predicted maximum energy product, $(BH)_{max}$, was generally correlated with the microstructure.

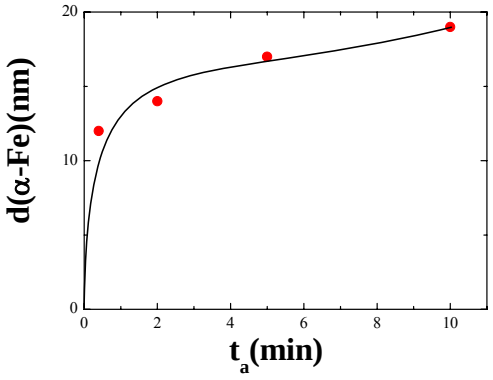

Fig.3 The mean α-Fe grain sizes as function of annealing time.

The $Nd_5Fe_{67}Cr_8Nb_2B_{18}$ nanocomposites were obtained by melt-spinning. In as obtained state, these were amorphous. The thermal treatment, at 650 ^oC, leads to the crystallization of the alloys. Unlike other systems having high boron content, for a relatively short annealing time ($t \leq 10$ min), only the presence of α–Fe was found. This can be correlated with high chromium content of the samples [7]. The mean dimensions of α–Fe crystallites increase rapidly for an annealing time smaller than 1 min and then a nearly linear variation was observed–Fig.3. A similar behaviour was shown for samples having related composition [8], For an annealing time $t_a \cong$ 10 min, the mean grain size of α–Fe is $\cong$ 19 nm.

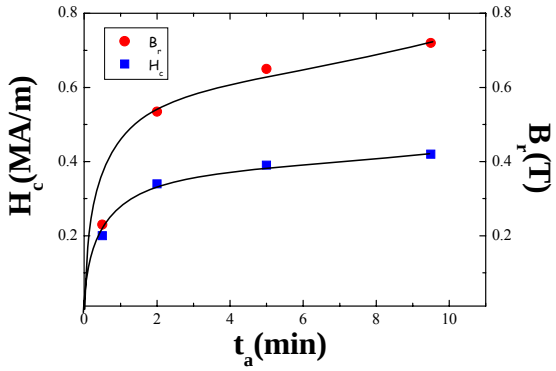

Fig.4. The remanent induction and coercive field as function of the annealing time.

As seen in Fig.4, the hard magnetic properties were developed when increasing annealing time, at 650 ^oC, up to 10 min. Both the remanent induction and the coercive field increase gradually with annealing time. The demagnetizing curve for a sample annealed during t_a=10 min, is shown in Fig. 5. The determined coercivity is $H_c \cong 0.42$ MA/m, higher than in case of $Nd_5Fe_{76.5}B_{18.5}$ sample, when a value of $\cong$ 0.3 MA/m was obtained [2]. The remanent induction is diminished, as compared to above mentioned sample, from $B_r \cong 1.2$ T to $\cong 0.73$ T. We conclude that the presence of chromium increases the coercive field, in parallel with the decrease of remanent induction. An energy product $(BH)_{max} \cong$ 98 kJ/m^3 was obtained. This is more than twice less than the predicted value. This reduction can be correlated with their microstructure. In the above samples, there is a distribution of the grain sizes around the mean values given in Fig. 3. Consequently, some α–Fe grains have dimensions greater than the exchange length, l_c. Thus, in addition to the exchange coupling between hard and soft magnetic phases there are dipolar interactions between grains [9]. The effect of dipolar interactions on the magnetic properties of nanocomposite magnets has been analysed by micromagnetic simulations [10]. The dipolar interactions play an important part, during demagnetization process, particularly in samples having high iron content

and larger dimensions than l_c. In this case, there can be exchange induced magnetization reversal near the grain boundaries and a low nucleation field of soft magnetic phase, respectively.

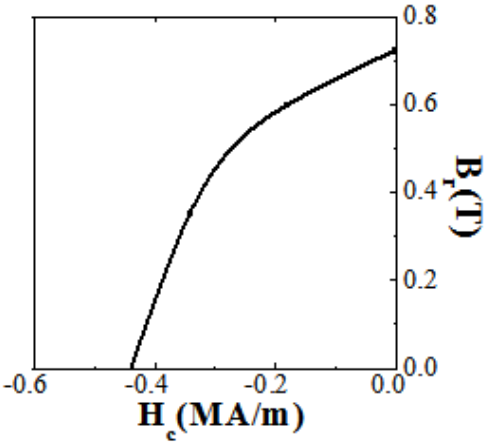

Fig. 5.The demagnetization curve for $Nd_5Fe_{67}Cr_8Nb_2B_{18}$ alloy, thermally treated at 650^0C, during 10 min.

3. Magnetic properties of Nd–Fe–Co–Al–B system

The $R_2Fe_{14}B$ compounds, where R is a rare–earth crystallize in a tetragonal structure $P4_2/mnm$ space group. In this structure the iron atoms are located in six different sites, the rare–earth in two and boron in one type of sites. In this structure, the distances between iron atoms cover a large range of values. The exchange interactions between iron atoms situated at distances $d_{FeFe} < 2.50$ Å are negative. Shorter d_{FeFe} values than above, were evidenced between j_1–k_2 and j_1–j_1 iron sites. The exchange interactions between iron atoms situated at greater distances are positive and stronger than negative ones and consequently the negative exchange interactions are not satisfied. A large magnetic energy is stored which brings about the low ordering temperatures. Thus, the Curie temperatures of $Nd_2Fe_{14}B$ is only 54 % from that of pure iron. Consequently, at room temperature, T_{RT}, where $T_{RT}/T_c \cong 0.50$, significant variations of the magnetic characteristics of permanent magnets based on this compound is shown, particularly of coercive field.

The magnetic properties of Nd–Fe–B permanent magnets, where the hard magnetic phase is $Nd_2Fe_{14}B$, can be improved by increasing the coercive field and Curie temperatures. A possible way to increase the anisotropy and coercive fields is the partial substitution of iron by aluminium [11,12]. The highest effect on the Curie temperatures is the replacement of iron by cobalt [13]. Taking the above into account we analysed the effect of coupled substitutions of iron by cobalt and aluminium. Firstly, we discuss the magnetic properties of the hard magnetic phases, $Nd_2Fe_{14-x-y}Co_xAl_yB$, in which small amounts of iron were replaced by aluminium ($y \leq 1$) and cobalt ($x \leq 2$). Then, we analyse the magnetic properties of $Nd_5Fe_{77-x-y}Co_xAl_yB$ sintered magnets. The effect of aluminium substitution on the coercive field of $Nd_{15}Fe_{77-y}Al_yB_8$ alloys will be particularly discussed.

3.1 $Nd_2Fe_{14-x-y}Co_xAl_yB$ compounds

The $Nd_2Fe_{14-x-y}Co_xAl_yB$ compounds with $x \leq 2$ and $y \leq 1$ were prepared by melting the consistent elements in a water–cooled copper boat by rf heating under following ultra high purity argon [11]. The samples were annealed for two weeks, at 950 ^{o}C, and then rapidly cooled to room temperature. The X-ray analyses showed that the compounds crystallize in a tetragonal structure of $P4_2/mnm$ type.

The composition dependences of the Curie temperatures, T_C, are given in Fig. 6. The T_C values increase, in mean, by ≅67 K when one iron atom is replaced by cobalt and decrease by ≅ 70 K when one iron atom is substituted by aluminium. The above behaviour can be correlated with the site occupancy of the atoms in $P4_2/mnm$ type lattice. The cobalt atoms, nearly randomly substitute iron in k_1, k_2, j_1 and c sites [2]. As a result, the negative exchange interactions connected with the presence of iron in j_1 and k_2 sites are gradually diminished when the cobalt content increases. In addition, strong iron–cobalt–exchange interactions are present. The Curie temperatures, thus increase significantly. The aluminium substitution occurs first for j_2 type sites up to one atom and further replace the iron in c sites [2]. In our experimental study we limited the maximum aluminium content to y=1 and consequently we suppose that all the aluminium is located in the j_2 positions. The Curie temperatures will decrease since Al replace Fe in sites involved in positive exchange interactions, as a result of magnetic dilution effects, as well as of the Fe3d–Al2p band hybridizations of the iron atoms situated in the first coordination shell to an aluminium one. Also the iron in j_2 sites has a higher magnetic moment than the mean iron moments [2,14]. These effects strongly influence the saturation moment per formula unit. The magnetization decreases with a slope of ≅ 2.5 μ_B/Al atom, at room temperature–Fig.7.

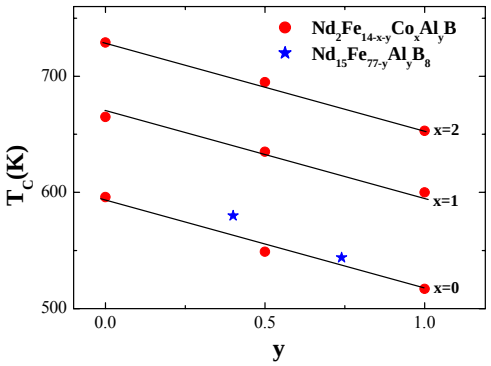

Fig. 6.The composition dependences of the Curie temperatures in $Nd_2Fe_{14-x-y}Co_xAl_yB$ compounds. The data for some $Nd_{15}Fe_{77-y}Al_yB_8$ alloys are also plotted.

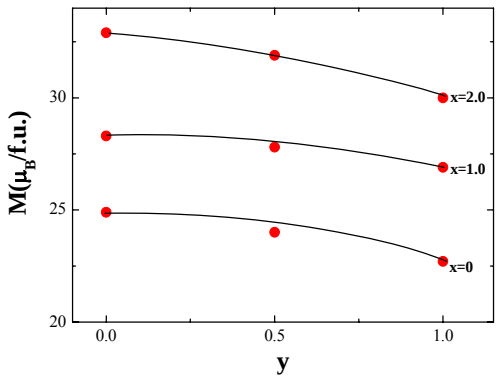

Fig. 7. The composition dependences of the magnetization, at room temperature, for $Nd_2Fe_{14-x-y}Co_xAl_yB$ compounds .

In case of $R_2Fe_{14-x}Co_xB$ system, there is a small increase of the magnetization, at 4.2K, when increasing cobalt content with a maximum situated in the composition range $1.5 \leq x \leq 2.0$ [2,13]. This behaviour is reminiscent to those characteristic of Fe–Co based alloys [15]. At room temperature, since of thermal effect, there is an apparent higher increase of the magnetization when iron is replaced by cobalt.

The composition dependences of the anisotropy fields in $Nd_2Fe_{14-x-y}Co_xAl_yB$ are shown in Fig.8. The value obtained for $Nd_2Fe_{14}B$, of $H_a \cong 6.8$ kOe, is in good agreement with that previously reported [16]. The anisotropy fields increase by ≅ 10 %, when the 0.5 Al atoms are present in lattice and then decrease. The presence of cobalt diminishes generally the anisotropy fields but the observed differences are relative smaller in the composition range $0 \leq x \leq 2$. The observed H_a values, at room temperature, are determined by two opposite mechanisms. The first one, is the decrease of the anisotropy field when increasing cobalt content. The second one is generated by the increase of the Curie temperature which leads to a smaller temperature dependence of the H_a values.

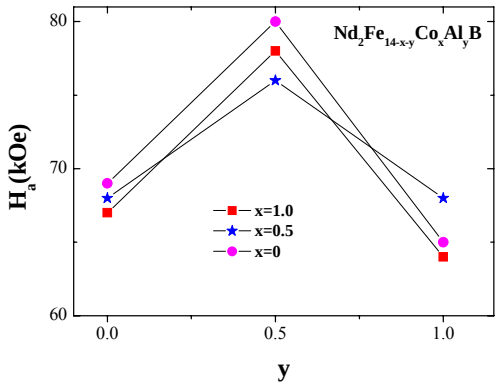

Fig. 8. The composition dependences of the anisotropy field , at room temperature, in $Nd_2Fe_{14-x-y}Co_xAl_yB$ compounds.

We can conclude that the properties of the Nd–Fe–Co–Al–B hard magnetic phases are strongly dependent on composition, which can be correlated with the site occupancy of substitution in tetragonal lattice.

3.2 Nd–Fe–Al–Co permanent magnets

Previously [12], was shown that the presence of aluminium increases significantly the coercive field of $Nd_{16}Fe_{76-y}Al_yB_8$ permanent magnets. In addition, was reported a diminution of the energy product as result of aluminium substitution.

In order to obtain further information on the matter we analysed the effect of aluminium on the coercivity in $Nd_{15}Fe_{77-y}Al_yB_8$ permanent magnets with $y \leq 4$. The anisotropic magnets were prepared by melting the constituent elements in an induction furnace, under purified argon atmosphere. The samples were crushed and powdered by ball milling. The dimensions of the grains were in the range of 2–4 μm. The powders were aligned in a magnetic field of 8 kOe and pressed. The sintering was performed at 1100 °C. A post sintering thermal treatment, at 580 °C, was also performed. The magnetic properties were determined at room temperature.

The demagnetizing curves of $Nd_{15}Fe_{75}Al_2B_8$ and $Nd_{15}Fe_{77}B_8$ magnets are plotted in Fig.9. The remanent induction decreases, and the coercive field increases in the aluminium doped sample. For the analysed samples with y=2 and y=4, if all aluminium entered in $P4_2/mnm$ type lattice, this will correspond to 2.6 % and 5.2 % of substituted iron. In a hard magnetic phase the respective content is equivalent to 0.37 and 0.73 iron atoms replaced by aluminium.

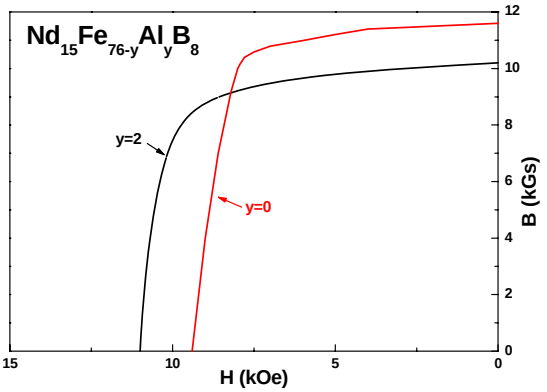

Fig. 9.The demagnetizing curves for $Nd_{15}Fe_{75}Al_2B_8$ and $Nd_{15}Fe_{77}B_8$ permanent magnets.

The Curie temperatures of the above samples are somewhat higher than those of the corresponding $Nd_2Fe_{14-y}Al_yB$ phases, having the same Al content as seen in Fig. 6. This suggests that not all aluminium entered in lattice and also the neodymium rich phase contained aluminium in their composition.

The composition dependence of the coercive fields in $Nd_{15}Fe_{77-y}Al_yB_8$ alloys are plotted in Fig.10. On the same

figure are given also the data reported by Zhang *et al.* [12]. Although the determined values follow the trend previously reported, these are in the mean by 1.5 kOe smaller. Both sets of data confirm the benefic effect of aluminium on the coercive field.

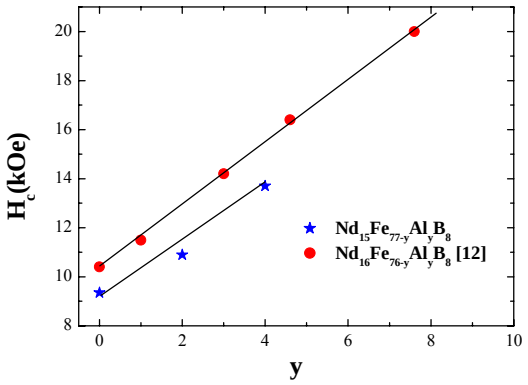

Fig. 10. Composition dependence of the coercive field in $Nd_{15}Fe_{77-y}Al_yB_8$ alloys as well as the data obtained in case of $Nd_{16}Fe_{76-y}Al_yB_8$ system [12].

A decrease of the melting temperature of Nd–rich phase was shown when the aluminium content is higher. As a result, there is an increase of the wettability of the Nd–rich phase, during sintering, and thus a better magnetic isolation of the hard magnetic grains. The more effective coating of the hard matrix grains will contribute to a significant increase of the coercivities. In addition, probably there is also a reduction of the lattice distortion induced by milling , and a smoothing of the roughness of the grain boundaries. According to Legras et al [17], two ternary compounds are the main constituents of the Nd–rich phase. These are δ–phase, $Nd_{30}Fe_{70-x}Al_x$ with $7 < x < 25$ and μ–phase $Nd_{33}Fe_{67-x}Al_x$ with $2.5 < x < 5$. When increasing the aluminium content it is expected that the above phases will be more rich in aluminium, and a reduction of melting temperatures is expected, as experimentally observed.

We note that high coercivities were obtained also in Nd–Fe–Al amorphous alloys [18]. In addition to the already proposed mechanisms for the coercivities, we believe that a better isolation of hard magnetic grains by other phases containing aluminium contribute also to the increase of the coercivity.

We prepared also an isotropic permanent magnet having the composition $Nd_{15}Fe_{71}Co_4Al_2B_8$. The coercive fields was H_C=8 kOe, although the Curie temperature increased up to $T_C \cong 650$ K.

We conclude that by using a suitable balance between Co and Al content substituting iron, magnets with suitable coercive fields and Curie temperatures can be obtained.

4. R–Fe–C Compounds

The preparation of $R_2Fe_{14}C$ compounds with light rare–earths, R, requires annealing treatment of as cast alloy in a fairly narrow temperature range [19]. The high temperature limit of this interval is determined by the solid state transformation of $R_2Fe_{14}C$ compounds into $R_2Fe_{17}C_x$ phases. The low temperature limit is less sharp and originates from the slow reaction kinetics that prevents complete conversion of the initial crystallization product into $R_2Fe_{14}C$ compounds. In order to increase the temperature range in which $Nd_2Fe_{14}C$–based compounds are formed, we replaced a fraction of carbon by boron as already suggested [20]. Thus, in case of $Nd_2Fe_{14}C_{0.8}B_{0.2}$ compounds, the high temperature limit, for thermal treatment, can be extended up to $\cong 1000\ ^oC$.

The $Nd_2Fe_{14-x}M_xC_{0.8}B_{0.2}$ with M = Ni, Cu, Al and $x \leq 1$ were obtained by melting the constituent elements in an induction furnace. The samples were thermally treated one week at 960 ^oC. The samples were nearly pure, the estimated impurity content being of the order of 6%.

Magnetic measurements were performed in large temperature range and fields up to 70 kOe. Some magnetizations isotherms are plotted in Fig.11. There is a decrease of magnetizations when iron is replaced by Al,Cu or Ni. The highest variation can be seen in aluminium doped samples. The analysis of magnetization curves showed that generally, the anisotropy decreased as result of the substitutions.

We performed a comparative analysis of the magnetic properties of $Nd_2Fe_{14-x}Cu_xA$ samples with A = B or $C_{0.8}B_{0.2}$–Fig.12. Both the Curie temperatures and saturation magnetizations are somewhat smaller than in corresponding boron compounds, although the anisotropy seems to be higher.

The $Nd_2Fe_{14-x}M_xC_{0.8}B_{0.2}$ compounds are ferromagnetically ordered. The substitutions of Fe by M elements, decrease the saturation magnetization, M_s, at 4.2 K. The M_s values are smaller than those expected from simple dilution model, particularly in aluminium substituted samples. This can be attributed to the hybridization of Fed and Alp bands.

The Curie temperatures increase when Fe is replaced, in small quantities, by Cu or Ni, and decrease as result of aluminium substitution. This fact can be correlated with peculiarities of crystal structure. In $R_2Fe_{14}C$ systems, as in $R_2Fe_{14}B$ compounds, the increase of Curie temperatures when Fe is replaced by Cu and Ni can be correlated with their possible distribution in Fe sites involved in negative exchange interactions [21].

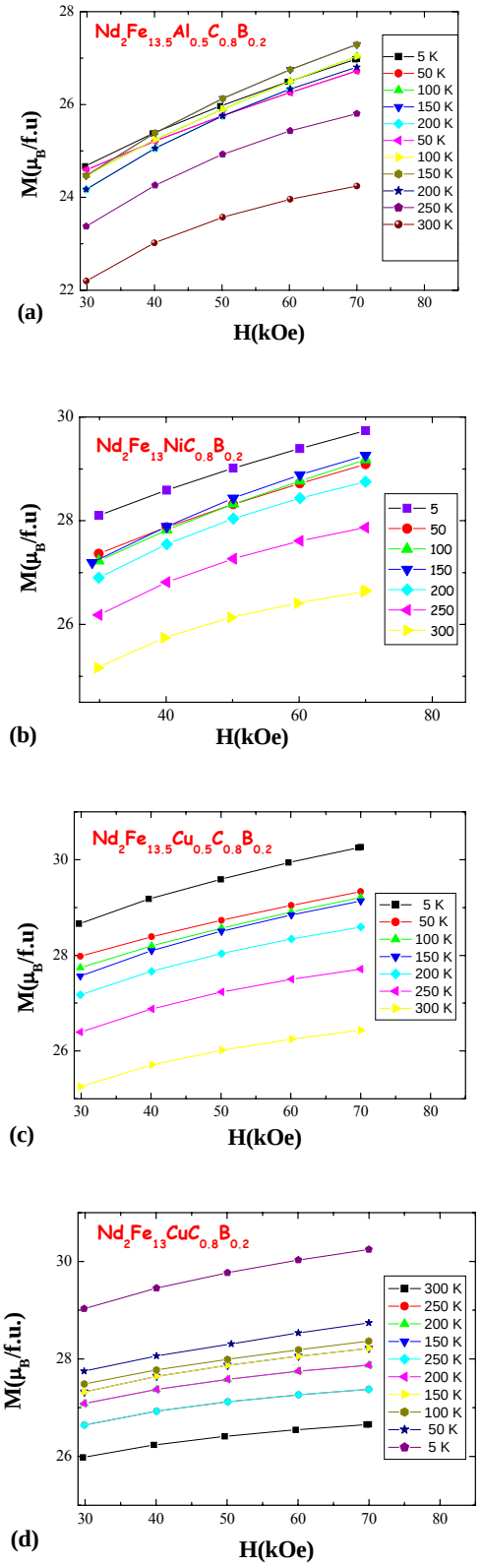

Fig. 11. Magnetization isotherms of $Nd_2Fe_{13.5}Al_{0.5}C_{0.8}B_{0.2}$ (a) $Nd_2Fe_{13}NiC_{0.8}B_{0.2}$ (b), $Nd_2Fe_{13.5}Cu_{0.5}C_{0.8}B_{0.2}$ (c) and $Nd_2Fe_{13}CuC_{0.8}B_{0.2}$ (d) compounds.

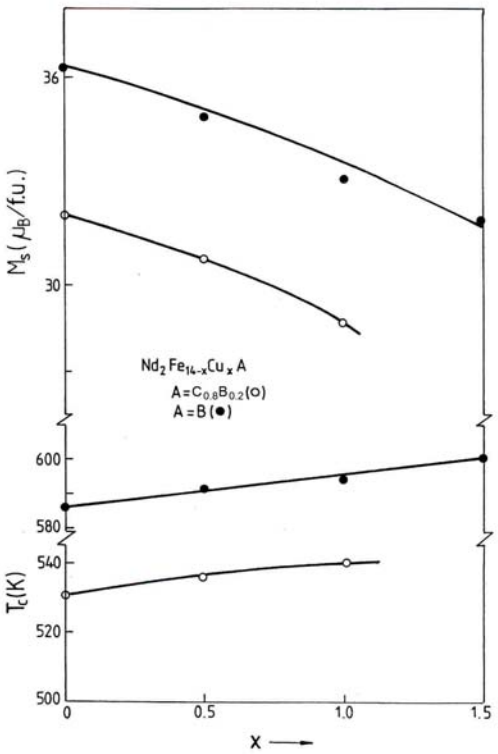

Fig. 12. Composition dependences of the saturation magnetization and of Curie temperatures in $Nd_2Fe_{14-x}Cu_xA$ compounds with A=B and $C_{0.8}B_{0.2}$..

We conclude that in $Nd_2Fe_{14-x}M_xC_{0.8}B_{0.2}$ compounds, the Curie temperatures are determined by site distribution of M elements. The saturation magnetizations are predominantly influenced by the nature of M element as well as their content.

We prepared also a $Nd_{15}Fe_{77}(C_{0.8}B_{0.2})_8$ sample. After thermal treatment at 950 ^oC, for three days, a coercive field of ≅ 4.5 kOe was shown. This value is only somewhat smaller than that obtained previously in $Nd_{16}Fe_{75}(C_{0.95}B_{0.05})_9$ sample [20], but sensitive smaller than in Nd-Fe-B magnets

5. Nanocrystalline soft magnetic materials

The wide range of applications of soft nanocrystalline and amorphous materials arise from their versatile nature. These alloys can be prepared without stoichiometric restrictions by melt spinning followed by a thermal treatment. For technical applications are of interest alloys having high saturation induction, B_s and highest possible permeability which provide fast magnetization reversal and low magnetic losses.

The above requirements can be obtained in iron based nanocrystalline alloys. Among them, the Finemet alloys, Fe–Si–B–Nb–Cu, are characterized as having ultra soft properties [22]. These alloys are obtained by splat cooling,

as amorphous samples, followed by recrystallization treatment at ≅ 500 °C. The nanocrystalline structure is essentially connected with the presence of Cu and Nb and their small solubility in bcc FeSi grains. After the recrystallization process was thermally activated, the copper atoms tend to be concentrated as clusters of nanometer sizes. The iron atoms are expelled from such copper zones. The regions having iron concentrations constitute the nucleation sites for α–FeSi grains. The increase of the grain dimensions is limited by the presence of Nb atoms, expelled from grains and located in amorphous phase. Boron is used to facilitate the formation of amorphous phase. Finally the alloy is constituted from bcc grains, having d≅15 nm dimensions, homogeneously distributed in the volume and separated by a FeNbBCu matrix. The maximum crystalline fraction of the alloy is 80 %.

The quasistatic hysteresis cycles for two samples having composition $Fe_{73.5}Si_{13.5}B_9Nb_3Cu_1$ are given in Fig.13 [23]. The coercive field is very low, of the order of 0.7 A/m.

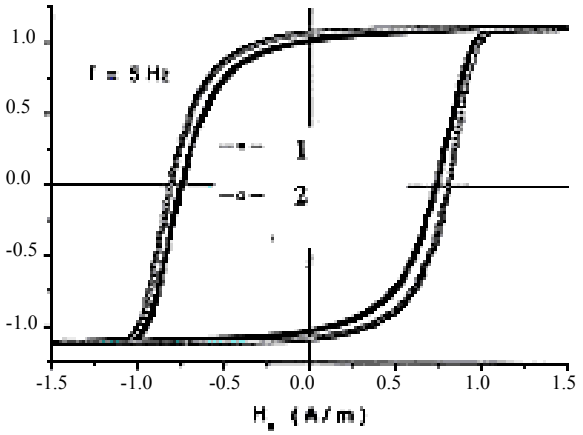

Fig. 13. Hysteresis loops of two nanocrystalline $Fe_{73.5}Si_{13.5}B_9Nb_3Cu$ samples.

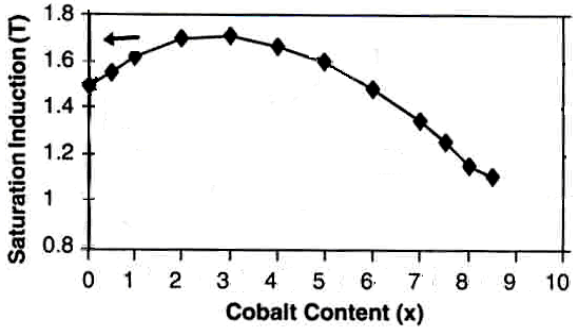

Fig. 14. Saturation induction for $Fe_{83-x}Co_xNb_7Si_1B_8Cu_1$ alloys [24].

The Finemet alloys have saturation induction B_s≅1.2 T. Efforts to increase the saturation induction have been made by adding cobalt. The magnetic properties of $Fe_{83-x}Co_xNb_7B_8Cu_1Si_1$ alloys are plotted in Fig.14 [24,25]. The highest B_s value was obtained for a sample with x = 3, namely B_s≅1.7 T. The primary phase, in nanocrystallized alloys, was based on α–FeCo. Although the saturation induction increase, the coercive fields are higher than in sample without cobalt. For a sample with x=3 a value H_C = 5.9 A/m was obtained. The magnetic anisotropy for compositions x<3 was attributed to nanoparticles structure, as being predominantly formed from bcc Fe and bcc CoFe [24].

6. Magnetocaloric materials having large relative cooling power

The magnetocaloric effects (MCE), in a large variety of magnetic materials, have been intensively studied in the last years, in connection with their use in magnetic refrigeration. The studies were correlated mainly with the magnetic phase transitions [26,27]. The entropy change, ΔS, was followed in materials which show both first order and second order phase transitions, respectively. The adiabatic temperature change was shown to be proportional to the partial derivative of the magnetization, M, with respect to temperature. Higher entropy changes were present in systems which show first order-type transition. In this case the main contribution to MCE comes from the change of the exchange interaction energy [26]. These materials may have hysteretic properties, which deteriorate MCE under the cycle of magnetization/demagnetization process. Consequently, the directions of researches were directed on materials having second order phase transition.

The magnetocaloric effect can be correlated also with a high temperature dependence of the rare-earth sublattice magnetizations in transition metal compounds. Consequently, we studied the $(Gd_xY_{1-x})_{n+1}Co_{3n+5}B_{2n}$ samples, having n = 2 and 3. Magnetic measurements were performed in the temperature range 4.2-700 K and fields up to 70 kOe [28,29].

The $(Gd_xY_{1-x})_3Co_{11}B_4$ and $(Gd_xY_{1-x})_2Co_7B_3$ compounds for x ≥ 0.2, are ferrimagnetically ordered, the gadolinium and cobalt magnetizations being antiparallely oriented. As example, in Fig. 15 we plotted the thermal variations of the resultant magnetizations for $(Gd_{0.6}Y_{0.4})_3Co_{11}B_4$ and $(Gd_{0.8}Y_{0.2})_2Co_7B_3$ compounds. By using a two sublattice molecular field model [30] we determined the exchange interaction coefficients N_{ij}, inside and between the magnetic sublattices. As example, for $(Gd_{0.6}Y_{0.4})_3Co_{11}B_4$, values $N_{Co\text{-}Co}$ = 150, $N_{Gd\text{-}Co}$ = -22 and $N_{Gd\text{-}Gd}$ ≅ 2 were obtained. As a result, we computed the thermal variations of gadolinium and cobalt magnetizations. Rather high variations, as function of temperature, are shown for gadolinium magnetizations, particularly in the intermediate temperature range.

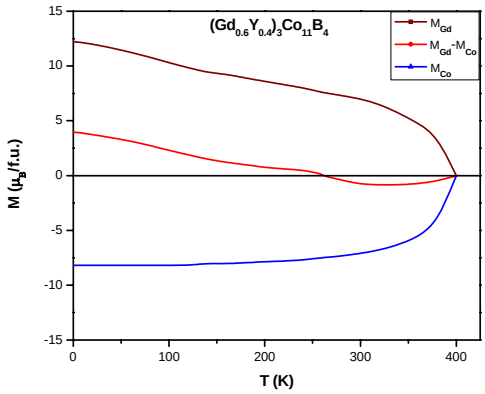

(a)

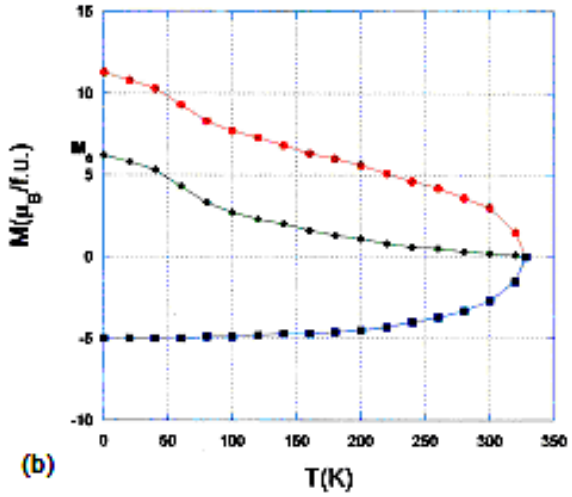

Fig. 15. Thermal variations of resultant and sublattices magnetizations in $(Gd_{0.6}Y_{0.4})_3Co_{11}B_4$ (a) and $(Gd_{0.8}Y_{0.2})_2Co_7B_3$ (b) compounds.

The entropy changes, ΔS, were computed from magnetization isotherms according to Maxwell relation:

$$\Delta S(T;0 \rightarrow H) = \int_0^H \left(\frac{\partial M}{\partial T}\right)_H dH \qquad (1)$$

From magnetization data, performed at constant temperature, and successive values of the applied field, H, the Maxwell equation can be approximated by the relation [31,32]:

$$\Delta S = \sum_i \frac{M_{i+1} - M_i}{T_{i+1} - T_i} \Delta H_i \qquad (2)$$

We denoted by M_{i+1} and M_i, the magnetizations measured in a field H, at temperatures T_{i+1} and T_i, respectively.

The computed entropy changes, ΔS, are plotted in Fig. 16 for the $(Gd_{0.6}Y_{0.4})_3Co_{11}B_4$ and $(Gd_{0.8}Y_{0.2})_2Co_7B_3$ compounds. In the last case the ΔS values were given only in the temperature range 8-150 K. Maxima values of $|\Delta S|$=6.2 J/kg K was shown at 100 K in $(Gd_{0.6}Y_{0.4})_3Co_{11}B_4$ and of 7.1 J/kg K at 70 K, for $(Gd_{0.8}Y_{0.2})_2Co_7B_3$ sample. There is a change in sign of ΔS values at the compensation temperature.

The maxima in entropy changes, ΔS_m, for $(Gd_xY_{1-x})_3Co_{11}B_4$ system follow the sequence: ΔS_m (x=1)> ΔS_m(x=0.4)> ΔS_m(x=0.8)> ΔS_m (x=0.6)> ΔS_m (x=0.2).

The relatively high magnetocaloric effects, at temperatures smaller than the Curie points, can be correlated with a high temperature dependence of the resultant magnetization, essentially determined by that of gadolinium.

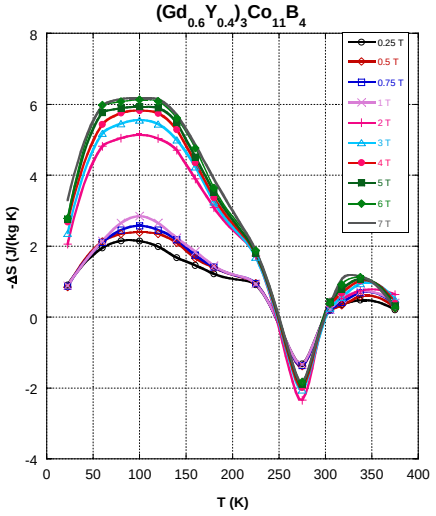

a

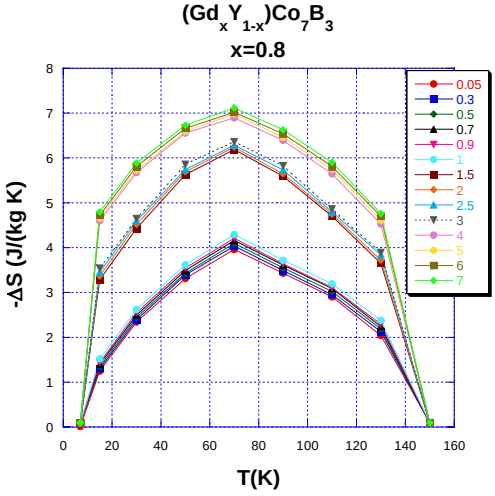

b

Fig.16 The entropy changes, ΔS, in $(Gd_{0.6}Y_{0.4})_3Co_{11}B_4$ (a) and $(Gd_{0.8}Y_{0.2})_2Co_7B_3$ (b)

A parameter characteristic for magnetocaloric materials is the relative cooling power, RCP(ΔS)= $|\Delta S_m|\delta T_m$, defined as a product of the maximum value of the entropy change $|\Delta S|$ and the full width at the half maximum, δT_m [31,32]. A large RCP(ΔS) value corresponds to a better magnetocaloric material. It was also suggested that more convenient for characterizing magnetocaloric materials is the specific renormalized cooling power, defined as RCP(ΔS)/ΔH, relative to external field variations, ΔH. In the above studied systems, there are very large RCP(ΔS) relative cooling powers, due to their large linewidth, δT_m. As a result, the RCP(ΔS)/ΔH values are higher than those observed in better magnetocaloric materials, which are somewhat smaller than 18 J/kg kOe [26]. There was shown to be a linear dependence of RCP(ΔS)/ΔH and the shift of the temperature at the phase transition [27]. The present data suggest that the above relation can be valid in the intermediate temperature range, centered at T_m, where maxima of $|\Delta S|$ values are shown.

6. Conclusions

Some types of magnetic materials were studied in correlations with their technical uses. The results obtained for hard Nd-Fe-Cr-Nb-B nanocrystalline alloy and Nd-Fe-M-C (M=Ni,Cu,Al) systems are given. The hard magnetic properties of Nd-Fe-B alloys are better than in case of Nd-Fe-C ones. In the Nd–Fe–Co–Al–B system, by using a convenable balance between Co and Al content substituting iron, magnets with large ranges of coercive fields and Curie temperatures can be obtained.

The Finemet type soft magnetic materials have low coercive fields. Although the addition of cobalt to the above alloys, increases the saturation magnetizations, there is also an increase of their coercivities and consequently of the magnetic losses.

High relative cooling powers can be obtained in ferrimagnetic R-Co-B based compounds. These were determined by the large temperature width at the half maximum of the entropy change. A correlation of the entropy changes with the temperature dependence of gadolinium sublattice magnetization was shown.

References

[1] M. Sagawa, S. Fujimura, M. Tagawa, H.Yamamoto, Y. Matsuura, J. Appl. Phys. **55**, 2083 (1984)

[2] E. Burzo, Rep. Progr. Phys. **61**, 1099 (1998) and references

[3] J. F. Herbst, Rev. Mod. Phys. **63**, 819 (1991) and references

[4] E. Burzo, E. Oswald, M. Q. Huang, E. Boltich, W. E. Wallace, Proc. 8th Int. Workshop on Rare-Earth Magnets and Their Applications, Dayton, 1985, p. 711; E. Burzo, E. Burzo, E. Oswald, M. Q. Huang, E. Boltich, W. E. Wallace, J. Appl. Phys. **57**, 419 (1985); E. Burzo, J. Optoelectron. Adv. Mater. **10**, 750 (2008).

[5] R. Coehorn, B. D. De Mooji, J. P. W. B. Duchateau, K.H.J. Buschow, J. Phys. **49**, C8-669 (1998).

[6] E.F. Kneller, R. Hawing, I.E.E.E. Trans. Magn. **27**, 3588 (1991)

[7] S. Hirosawa, H. Kanekiyo, Proc. 13th Int. Workshop on Rare-Earth Magnets and Their Applications, 1993, p. 87

[8] E. Burzo, C. Djega-Mariadassou, in Nanoscale Devices, Fundamentals and Applications, Springer Verlag, 2006, p. 371

[9] A. M. Gabay, M. Marinescu, G. C. Hadjipanayis, J. Appl. Phys. **99**, 08B506 (2006)

[10] C.B. Rong, H.W. Zhang, R.J. Chen, S.L. He, B.G. Shen, J. Magn. Magn. Mat. **302**, 126 (2006)

[11] E.Burzo, A.T.Pedziwiatr and W.E. Wallace, Solid State Commun. **61**, 57 (1987)

[12] M. Zhang, D.Ma, X.Jiang and S. Liu, Proc. 8th Int. Workshop on Rare – Earth Magnets and their Applications, Dayton, Ohio, 1985 p. 541

[13] E. Burzo, A.T. Pedziwiatr and W.E. Wallace, J. less Common Met. **111**, 83 (1985)

[14] E. Burzo, P. Vlaic , J. Optoelectron. Adv. Mater. **10**, 750 (2008)

[15] E. Burzo, Solid State Commun. **25**, 525 (1978)

[16] S. Hirosawa, Y. Matsuura, H. Yamamoto, S.Fujimura, M. Sagaw, H. Yamauchi, J. Appl. Phys. **59**, 873 (1986).

[17] L. Legras, J. Delmare, D.Lemarchand, J. Vu Dinh, P. Vigier, J. Alloys Compounds **218**, 17 (1985)

[18] A.Inoue, A.Takeuchi and T. Zhang, Metall. Matter. Trans. A **29**, 1779 (1998); J. Ding. Y.Li, X. Z. Wang, J. Phys. D. **32**, 713(1999)

[19] E. Burzo in Landolt Börnstein Handbuch, Vol. 19/i2, Springer Verlag, 1992, p. 237

[20] J. Eisses, B. D. De Mooji, K. H. J. Buschow, G. Martinek, J. Less Common. Met. **171**, 17 (1991)

[21] W. Kappel, E. Burzo and V. Pop, J. Magn. Magn. Mat. **157-158**, 35 (1996)

[22] Y. Yoshizawa, S. Ogawa and Y. Yamauchi, J. Appl. Phys. **64**, 6044 (1988)

[23] L. Fratila, Ph. D. Thesis, University Babes-Bolyai Cluj-Napoca and University J. Fourier, Grenoble, 2002

[24] Y. Yoshizawa and I. Ogawa, Proc. Intermag. Conf., Nagoya, Japan, 2005

[25] R. Hasegawa, J. Magn. Magn. Mat. **304**, 187 (2006).

[26] A.M. Tishin, J. Magn. Magn. Mat. **316**, 351 (2007).

[27] E. Brück, O. Tegus, D.T.C. Thanh, K. H. J. Buschow, J. Magn. Magn. Mat. **310**, 2793 (2007).

[28] R. Ballou, E. Burzo, V. Pop and A. Pentek, J. Appl. Phys. **73**, 5695 (1993).

[29] E. Burzo, V. Pop, C. Borodi and R. Ballou, I.E.E.E. Trans. Magn. **30**, 628 (1994).

[30] L. Néel, Ann. Phys. (Paris) **3**, 137 (1948).

[31] V. K. Pecharsky, K.A. Gschneidner Jr., J. Appl. Phys. **86**, 565 (1999).

[32] R. A. Gschneidner, V.K. Pecharsky, Ann. Matter. Sci. **20**, 387 (2000).

*Corresponding author:burzo@phys.ubbcluj.ro